Mechanistic investigations into the cyclopropanation of electron deficient alkenes with ethyl diazoacetate using [Co(MeTAA)]

Chirila, A.; Brands, M.B.; de Bruin, B.

DOI
10.1016/j.jcat.2018.02.013

Publication date
2018

Document Version
Final published version

Published in
Journal of Catalysis

Journal of Catalysis 361 (2018) 347–360

Contents lists available at ScienceDirect

Journal of Catalysis

journal homepage: www.elsevier.com/locate/jcat

Mechanistic investigations into the cyclopropanation of electron-deficient alkenes with ethyl diazoacetate using [Co(MeTAA)] ☆

Andrei Chirila, Maria B. Brands, Bas de Bruin *

Homogeneous, Supramolecular and Bio-Inspired Catalysis Group (HomKat), van 't Hoff Institute for Molecular Sciences (HIMS), University of Amsterdam, Science Park 904, 1098 XH Amsterdam, The Netherlands

ARTICLE INFO

Article history:
Received 21 January 2018
Revised 13 February 2018
Accepted 14 February 2018
Available online 30 March 2018

Keywords:
Metalloradical
Cyclopropanation
Kinetics
Mechanistic investigations
DFT
RPKA
Open-shell catalysis

ABSTRACT

A detailed mechanistic study of the cyclopropanation of electron-deficient alkenes, namely methyl acrylate with ethyl diazoacetate (EDA), was carried out, aiming at understanding both the superior activity and the higher sensitivity of the cobalt(II) tetramethyldibenzotetraaza[14]annulene [Co(MeTAA)] catalyst as compared with cobalt(II) tetraphenylporphyrin [Co(TPP)]. Cobalt(III)-carbene radicals were demonstrated to be present as key intermediates in the reaction, using a combination of kinetic studies, experimental EPR spin-trapping experiments, and supporting DFT studies. Reaction progress was monitored in real time by observing N_2 formation and measuring its partial pressure under isothermal conditions. Reaction progress kinetic analysis (RPKA) was used to analyze the experimental data. Results showed that the reaction is first-order in both [catalyst] and [EDA] and zero-order in [methyl acrylate], in agreement with the DFT-calculated mechanism. The calculated activation parameters corresponding to the rate-determining step of the reaction are in agreement with the experimental values, thus providing strong support for the proposed metalloradical mechanism.

1. Introduction

An attractive method for preparing functionalized cyclopropanes is the transition-metal-complex-catalyzed reaction of olefins with diazo compounds. Many catalytic systems, such as copper(I) or rhodium(II) complexes, have been applied successfully to the cyclopropanation of electron-rich olefins [1]. However, their catalytic activity toward electron-deficient olefins, such as acrylates, proved to be below par due to the electrophilic character of the Fischer-type metal–carbene complex intermediates typically involved in these reactions. This drawback has been solved by the introduction by the groups of Nakamura [2], Katsuki [3], and Zhang [4] of cobalt(II) complexes of salen and porphyrin ligands capable of both diastereo- and enantioselective cyclopropanation of electron-deficient olefins. This remarkable reactivity suggests a (more) nucleophilic character of the metal–carbene complex intermediate, which is not what one might expect from the reaction of late transition metals with diazo compounds. Formation of Fischer-type carbenes, stabilized by an ester group, would be expected for these systems, but their reactivity toward electron-deficient olefins reveals the contrary.

A few studies have aimed at explaining the unexpected behavior of cyclopropanation of electron-deficient alkenes using [Co^{II}(salen)] and [Co^{II}(por)] systems by performing mechanistic studies and attempting to isolate and detect intermediates. One of them was performed by Gallo, Cenini, and co-workers [5]. They investigated the cyclopropanation of styrene with ethyl diazoacetate (EDA) catalyzed by cobalt(II) tetraphenylporphyrin [Co(TPP)] by monitoring the reaction over time, using IR spectroscopy. The initial rates method, which is a steady state approximation method, was chosen for the kinetic studies. Therefore, the reaction was monitored with one of the components always present in large excess. Quite remarkably, the results indicated first-order rate dependence in [styrene], [EDA], and [catalyst]. However, the rate order in [styrene] proved complex and only at low styrene concentrations was first-order behavior observed. In another report from the same group [6], kinetic studies were performed in which [Co^{II}(salen)] was used as a catalyst for the cyclopropanation of α-methylstyrene and EDA. This time, first-order rate dependence was found for [EDA] and [catalyst], and zero-order for [α-methylstyrene].

Based on previous studies of Johnson [7], their kinetic studies, and using analytical tools such as IR and NMR, Cenini and co-workers proposed that two intermediate metal–carbene

☆ This paper is part of the thematic issue on "Mechanism of Molecular catalysis".

* Corresponding author.
E-mail address: b.debruin@uva.nl (B. de Bruin).

https://doi.org/10.1016/j.jcat.2018.02.013
0021-9517/

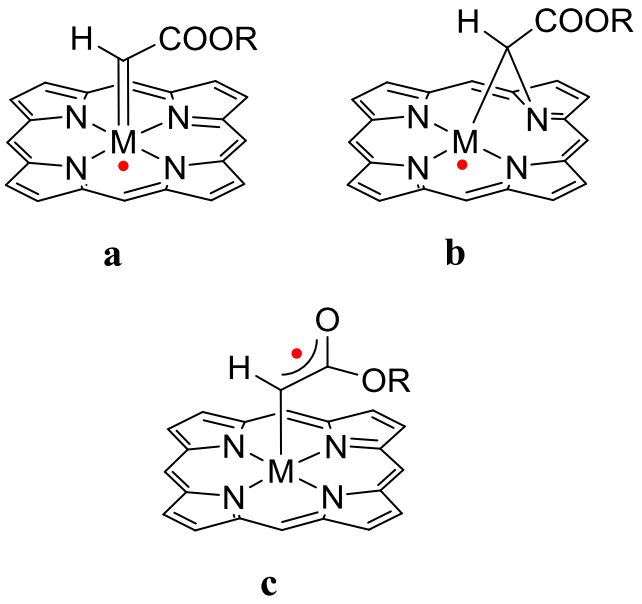

Fig. 1. Structures of the cobalt–carbene intermediates proposed in the studies of the groups of Cenini, Gallo, and Yamada [5,9].

complexes [Co(TPP)(CHCOOEt)] can be formed (Fig. 1a and b). The first, called "terminal carbene" a, is the more reactive species and was proposed to isomerize rapidly to form the "bridging carbene" species b via insertion of the terminal carbene into the Co—N bond of the porphyrin. A similar bridging carbene was also observed for [Co(salen)(CHCOOEt)] [8]. Neither of these metal–carbene complexes was considered to be the key cyclopropanation intermediates in the study of Cenini and Gallo, however. Based on the kinetic studies, the authors proposed that the EDA adduct [Co(TPP)(EDA)] reacts directly with styrene in the rate-limiting step [5] without prior formation of a metal–carbene complex. Any carbene complex formation was proposed to lead to carbene-dimerization side-product formation and catalyst deactivation [5].

Studies performed by Yamada and co-workers, on the other hand, showed formation of "terminal carbene" species for both [Co(salen)] and [Co(TPP)] [9]. However, the IR stretch frequency of the carbonyl group indicated a single-bond character for the cobalt–carbene bond. Therefore, Yamada proposed that single-electron transfer from cobalt to the carbon center occurs, leading to formation of a cobalt–carboxyethyl species in which the spin density is delocalized over the α-carbon atom and the carbonyl moiety, which would explain the surprising IR frequency detected experimentally (Fig. 1c).

Remarkably, the deactivated catalyst from the reaction medium in the form of [Co^{III}(TPP)(CH_2COOEt)] has been isolated and characterized using X-ray diffraction [5]. This is also an indication that the carbene intermediate species has "carbene radical" character, although the crystallographic evidence is only indirect. As a result of the radical character of the terminal carbene, hydrogen atom abstraction from the reaction medium (or EDA) occurs. To further shine light on the nature of the species involved, Zhang, de Bruin, and co-workers [10] decided to investigate the mechanism of [Co^{II}(por)]-catalyzed cyclopropanation of ethyl diazoacetate with methyl acrylate using a combination of EPR, ESI-MS, and DFT studies. The reported findings confirmed experimentally the presence of a redox noninnocent carbene ligand, which is formed upon reaction of EDA with the cobalt porphyrin. The EPR spectrum indicates the presence of both a "terminal carbene" showing a "carbene radical" character and a "bridging carbene" showing a cobalt radical character (Fig. 1b). DFT calculations revealed that these species are in dynamic equilibrium, with a low barrier to their interconversion. The DFT calculations further showed that cyclopropanation occurs via a stepwise radical process, involving formation of the terminal carbene radical species (Fig. 1c), which is the species reacting with the olefin. The DFT-calculated barriers for carbene radical formation and their reaction with the olefin were very similar, in agreement with first-order kinetics in both [EDA] and the [olefin] found by Cenini and Gallo, despite a stepwise reaction mechanism [10].

In our previous studies [11], we described the catalyst [Co(MeTAA)], which had never been used before as a carbene-transfer catalyst, but is much more active than [Co(TPP)] in the cyclopropanation of electron-deficient alkenes with diazo compounds. The reasons for the improved activity were not obvious, as the [Co(MeTAA)] complex has a structure very similar to that of [Co(TPP)] (Fig. 2). Hence, we wondered if the mechanism for olefin cyclopropanation with [Co(MeTAA)] is similar to the one reported for [Co(TPP)] or not, and what could be the reason for the enhanced activity of this complex. Therefore, we decided to investigate the reaction mechanism of [CoMeTAA]-catalyzed cyclopropanation of methyl acrylate, using ethyl diazoacetate as the carbene precursor. The results are described in this paper. Full-system DFT calculations including Grimme's dispersion corrections have been performed for both [Co(TPP)] and [CoMeTAA] to make direct comparison between the two systems possible. Spin-trapping experiments followed by detection by EPR proved a valuable tool in determining if the mechanism follows a radical-type pathway, and Blackmond's reaction progress kinetic analysis (RPKA) has been used to determine the rate law and to identify catalyst deactivation processes.

RPKA has been chosen over the more common initial rates method, in which an overwhelming excess of one or more reactants is used relative to the species of interest. With RPKA, the reaction is probed under synthetically relevant conditions at concentrations similar to the ones used when not exploring the rate law. In general, the mechanism can vary depending on both the relative and the absolute concentrations of the species involved. Therefore, more representative results of reaction behavior under commonly utilized conditions are obtained using this approach than by traditional kinetic studies using the initial rate approach.

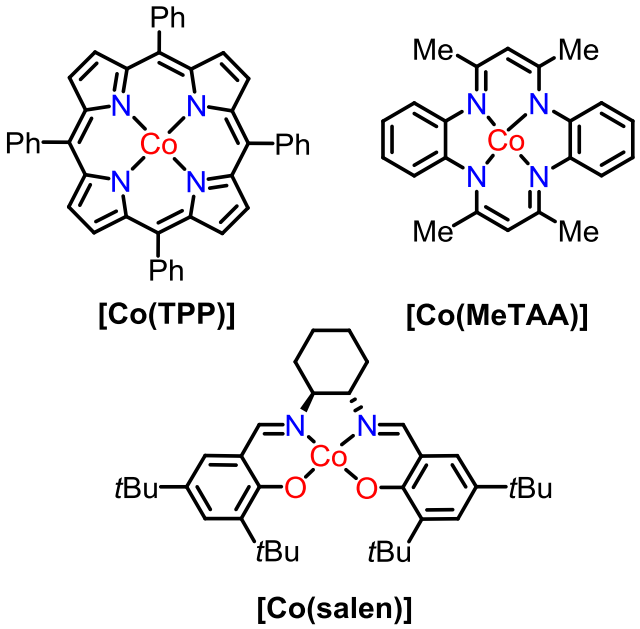

Fig. 2. Cobalt(II) complexes used as catalysts for cyclopropanation.

By measuring the reactions in their entirety and not just in the initial phases, unexpected behavior such as catalyst deactivation, product inhibition, or even changes in mechanism can be detected. Moreover, RPKA requires fewer experiments, is a faster method, and arguably is more accurate than traditional kinetic measurements [12].

2. Experimental

2.1. General details

Chemicals used during this research were purchased from Sigma Aldrich. Ethyl diazoacetate and methyl acrylate were degassed prior to use, via the freeze–thaw–pump method. Methyl acrylate was passed through basic alumina before use to remove stabilizers (radical scavengers). Both substrates were stored refrigerated (4 °C). The [Co(MeTAA)] catalyst is not commercially available and was synthesized according to a known procedure [13]. All reactions were performed under an inert atmosphere. Neslab ULT-80 was used as a cryostat for isothermal reaction conditions. The kinetic kit used for real-time pressure measurements was the X102 kit from the company Man on the Moon (Fig. 3).

2.2. General procedure for kinetic measurements

To the reaction flask was added a 1.0 cm cylindrical stirring bar, while all connections were checked for a leak-free system. Then the whole system was flushed with nitrogen. The order of addition of the reactants was as follows: First the catalyst solution, second the solvent, third the alkene, and finally the diazo compound. After addition of the first three reactants, the septum of the reaction flask was replaced and the whole reaction setup was introduced into the thermostatic ethanol bath. The reaction mixture was stirred at 500 rpm and cooled to the desired temperature for 30 min. A pressure/temperature measurement was started, and then the diazo compound was added at once and the reaction started. Once nitrogen evolution had ended, and the pressure was constant, data recording was stopped. Then the resulting mixture was concentrated and the residue purified by flash chromatography (silica gel) or extracted in pentane for analysis of the reaction products.

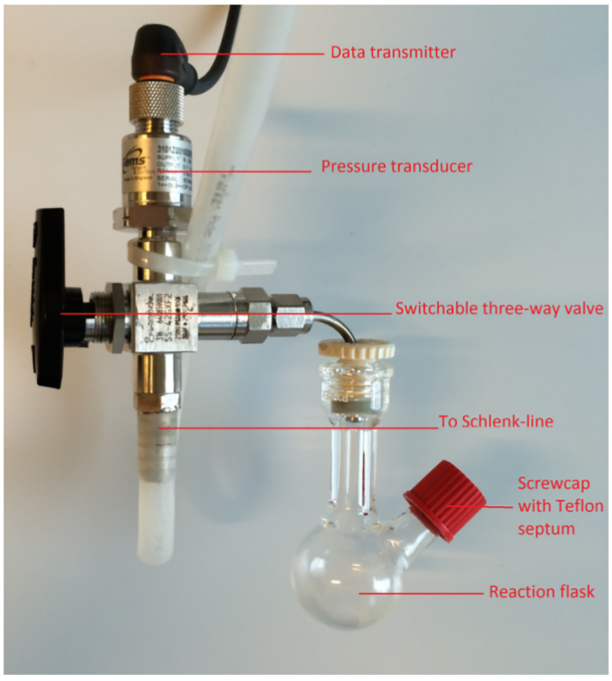

Fig. 3. Kinetic kit used for gas-release experiments.

2.3. Reaction details

The reaction took place in a flame-dried Schlenk flask (with a total gas volume of 20.1 mL) that was attached to a pressure/temperature sensor and placed in a thermostatic ethanol bath at 283 K. The volume of liquid reaction mixture was kept constant at 2 mL. The different conditions can be found in Table 1. A 0.01 M stock solution of [Co(MeTAA)] in toluene was used for all experiments. A 0.474 M cyclopropane stock solution in toluene was used. All reactions were performed in duplicate or triplicate, to ensure that the data were reproducible.

2.4. Characterization

Ethyl methyl 1,2-cyclopropanedicarboxylate (Fig. 4). *Trans*-isomer: ^{1}H NMR (400 MHz, $CDCl_3$) δ 4.06 (q, J = 7.1 Hz, 2H), 3.61 (s, 3H), 2.14–2.01 (m, 2H), 1.38–1.30 (m, 2H), 1.18 (t, J = 7.2 Hz, 3H). ^{13}C NMR (101 MHz, $CDCl_3$) δ 172.20, 171.65, 61.04, 52.09, 22.37, 22.08, 15.28, 14.13. HRMS (EI): Calcd. for $C_8H_{12}O_4$ m/z 172.0736; found m/z 172.0737. GC analysis: Supelco SPB-1 (temp program: initial temp = 70 °C, 7.00 °C/min, final temp = 250 °C, final time = 5.00 min) *trans*-isomer: t = 14.66 min, *cis*-isomer: t = 14.93 min.

2.5. Comparison of the kinetics between [Co(MeTAA)] and [Co(TPP)]

A preliminary study (Fig. 5) was performed to compare the reaction rates between [Co(MeTAA)] and [Co(TPP)]. There is a clear and remarkable difference between the two catalysts in the times required to reach full conversion (0.65 bar). For [Co(MeTAA)] this is achieved in less than 3 min, while for [Co(TPP)] only 50% conversion is reached after 45 min. However, full kinetic studies would be needed for the [Co(TPP)] system to fully compare reaction rates and establish additional mechanistic conclusions about the [Co(TPP)]-catalyzed reactions. This is, however, hampered by the solubility issues of [Co(TPP)] at 283 K. Running the kinetic experiments using identical reaction conditions is therefore impossible. Separate kinetic experiments could perhaps be performed for [Co(TPP)] using a higher reaction temperature, a different solvent, and lower catalyst concentrations to maintain homogeneity, but direct comparison with the kinetic data of [Co(MeTAA)] as reported in this paper is not possible.

2.6. Computational details

Geometry optimizations were carried out with the Turbomole program package [14] coupled to the PQS Baker optimizer [15] via the BOpt package [16]. We used unrestricted ri-DFT-D3 calculations at the BP86 level [17] in combination with the def2-TZVP basis set [18] and a small (m4) grid size. All minima (no imaginary frequencies) and transition states (one imaginary frequency) were characterized by calculating the Hessian matrix. ZPE and gas-phase thermal corrections (entropy and enthalpy, 298 K, 1 bar) from these analyses were calculated. The nature of the transition states was confirmed by following the intrinsic reaction coordinate.

DFT calculations without dispersion corrections strongly underestimate the metal–ligand interactions, as was clear from a series of test calculations. We therefore employed Grimme's version 3 (disp3) dispersion corrections. The computed dispersion-corrected metal–ligand association/dissociation energies to/from the nonsolvated [Co(TPP)] catalyst are overestimated, though. This is due to neglected dispersion interactions between the metal binding site of the catalyst and a solvent molecule in solution.

Table 1
Reaction conditions for RPKA.

Reaction	CoMeTAA	EDA	Methyl acrylate	Toluene	Cyclopropane
Standard conditions (1.5%)	750 μL 0.0075 mmol 0.015 eq	53 μL 0.5 mmol 1 eq	90 μL 1 mmol 2 eq	1100 μL	
Higher catalyst concentration (2%)	1000 μL mmol 0.02 eq	53 μL 0.5 mmol 1 eq	90 μL 1 mmol 2 eq	857 μL	
Lower catalyst concentration (1%)	500 μL 0.005 mmol 0.01 eq	53 μL 0.5 mmol 1 eq	90 μL 1 mmol 2 eq	1357 μL	
Same excess at 25% conversion	750 μL 0.0075 mmol 0.015 eq	40 μL 0.375 mmol 1 eq	79 μL 0.875 mmol 2.33 eq	1132 μL	
Same excess at 50% conversion	750 μL 0.0075 mmol 0.015 eq	29 μL 0.25 mmol 1 eq	68 μL 0.75 mmol 3 eq	1156 μL	
Same excess at 50% conversion with product addition	750 μL 0.0075 mmol 0.015 eq	29 μL 0.25 mmol 1 eq	68 μL 0.75 mmol 3 eq	629 μL	530 μL
Different excess	750 μL 0.0075 mmol 0.015 eq	53 μL 0.5 mmol 1 eq	135 μL 1.5 mmol 3 eq	1062 μL	

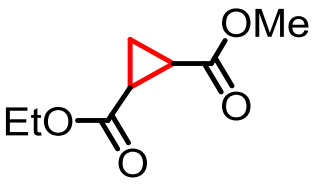

Fig. 4. Ethyl methyl 1,2-cyclopropanedicarboxylate.

We therefore used the van der Waals complex between [Co(TPP)] and a discrete toluene solvent molecule (interacting with the catalyst at the metal binding site) as the energetic reference point in our calculations to prevent overestimation of the metal–ligand interactions as a result of such uncompensated dispersion forces. However, this approach also leads to an erroneous cancellation of translational entropy contributions to the computed free energies. This is because the translational entropy contributions to substrate/product association/dissociation are fully counterbalanced by the translational entropy contributions resulting from dissociation/association of the involved solvent molecule in the DFT-calculated thermodynamics ([Co(TPP)(toluene)] + L ↔ [Co(TPP)(L)] + toluene). This is not realistic in comparison with actual solution phase chemistry, for which the translational entropy contributions associated with substrate/product association/dissociation steps can of course not be neglected [19]. Therefore, we applied a translational entropy contribution of -26 cal mol^{-1} K^{-1} to the computed free energies of all substrate/product binding/dissociation steps in the catalytic cycle. A similar approach was used in a recently published paper from our group [20].

3. Results and discussion

The study started with DFT geometry optimizations of the full reaction systems. The investigated reactions are the cobalt(II)-catalyzed cyclopropanation reactions of methyl acrylate and styrene, using EDA as the carbene precursor. Calculations for both [Co(MeTAA)] and [Co(TPP)] have been performed without any structural simplifications of the molecules involved. This allows for direct comparison of the two catalysts. The [Co(TPP)] optimizations from this work extend the previous reported calculations [10], in which the geometry optimizations were obtained using a lower-level basis set, without dispersion corrections and using

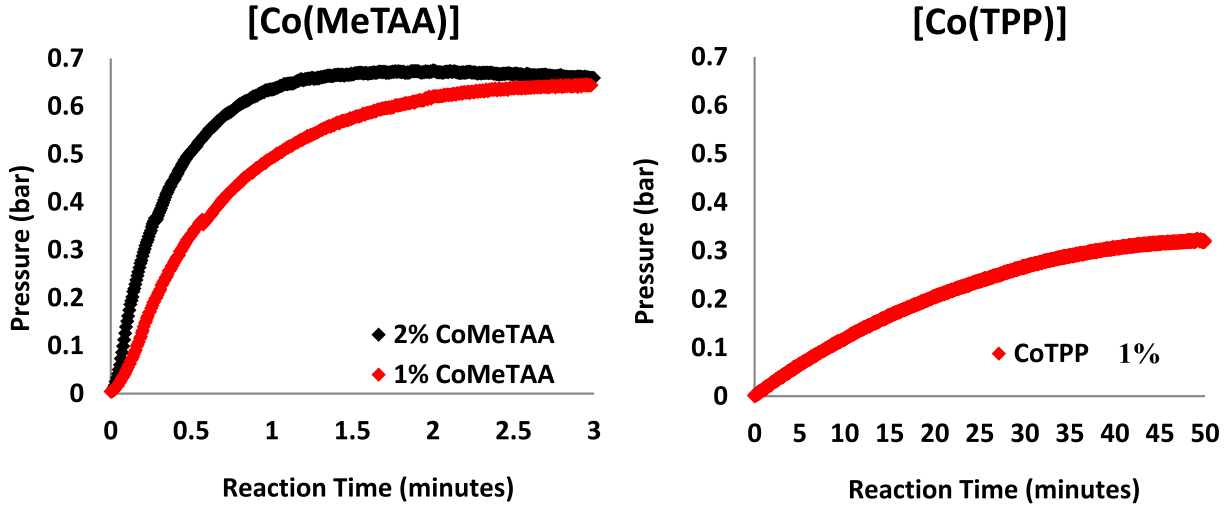

Fig. 5. Preliminary reaction rate comparison between the cyclopropanation of EDA and methyl acrylate, catalyzed by [Co(MeTAA)] and [Co(TPP)]

simplified molecular structures. In the present study, full atom structures, the BP86 functional, and the def2-TZVP basis were chosen, and the study includes Grimme's version 3 dispersion corrections.

The DFT calculations strongly suggest, as has previously been reported for [Co(TPP)], that the [Co(MeTAA)]-catalyzed reaction also proceeds via a stepwise radical addition–substitution pathway (Scheme 1). The key intermediates have an "organic radical" character. The first step (**I**) involves the interaction between [Co(MeTAA)] **A** and EDA to form the transient intermediate **A'**, which loses dinitrogen during step **II**. This leads to the formation of a carbon-centered radical terminal carbene, **B**, that is in equilibrium with the bridging radical carbene **E**. The terminal carbene is best described as a one-electron reduced Fischer-type carbene [21]. The bridging radical carbene **E** is a dormant state of the catalyst and is incapable of forming cyclopropane. The third step in the cycle (**III**) is irreversible radical addition of the carbene radical **B** to methyl acrylate, forming the γ-radical **C** species. The γ-radical species **C** then easily cyclizes to form the corresponding product during step **IV**, while the catalyst returns in its original state. This last step is a concerted radical type C—C bond formation with simultaneous homolysis of the Co—C bond. The barrier of this ring-closure reaction is so low that cyclopropane formation is the only favored reaction pathway, no other pathway, such as addition of another molecule of acrylate, being possible. All attempts to react the diazo adduct complex **A'** directly with the olefin, as has been proposed by Cenini and Gallo [5], were unproductive.

Analysis of the initial state of the catalyst is performed in Fig. 6. The energy differences between different species reveal that the toluene adduct of [Co(MeTAA)] is the most stable species in solution. Several modes of coordination of EDA to the catalyst are possible. However, their energies are 4.3–5.3 kcal mol^{-1} higher (Fig. 6, left). For [Co(TPP)], the energies of these species are even higher, ranging from 5.8 to 9.7 kcal mol^{-1} above those of the toluene adduct of the complex (Fig. 6, right).

The calculated free energies for the cyclopropanation steps mediated by [Co(MeTAA)] are shown in Fig. 7. The first step is activation of the ethyl diazoacetate by [Co(MeTAA)] with release of dinitrogen. This step has a transition state barrier **TS$_1$** of +14.5 kcal mol^{-1}, the highest of all reaction steps in the cyclopropanation

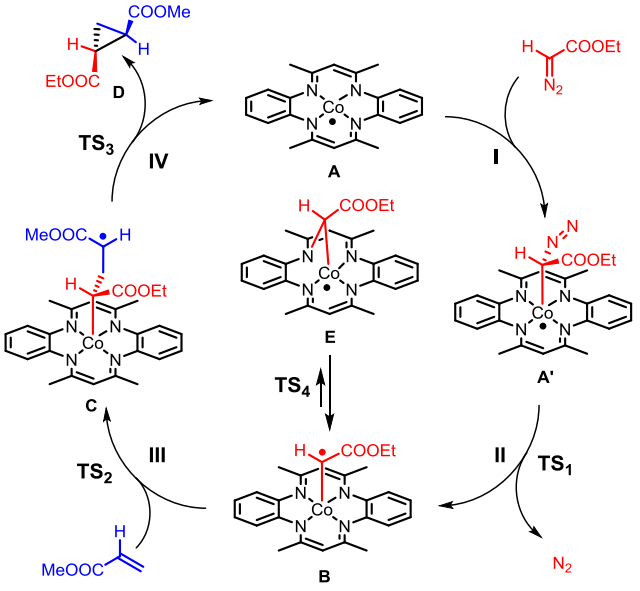

Scheme 1. Proposed mechanism of the [CoMeTAA]-catalyzed cyclopropanation of methyl acrylate with ethyl diazoacetate.

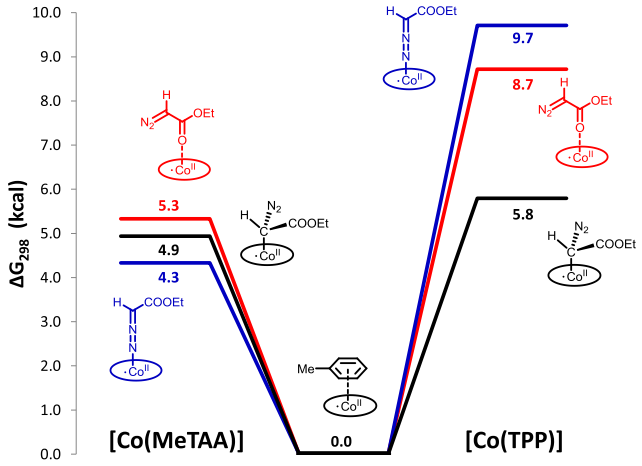

Fig. 6. Energy diagram—substrate coordination to [Co(MeTAA)] and [Co(TPP)].

cycle, thus suggesting that this is the rate-determining step. Formation of the carbene radical **B**, with release of nitrogen, is exergonic. In contrast to the [Co(TPP)] mechanism (Figs. 8 and 9), the species **B"** has a much lower energy than the bridging carbene **E"**. The latter was observed in previous studies [10] to be the resting state species of the [Co(TPP)]. This is clearly not the case for the [Co(MeTAA)] catalyst, as conversion of **B** to **E** is associated with a high **TS$_4$** barrier of +19.6 kcal mol^{-1}, which is much higher than the barrier for reaction of **B** with the acrylate (**TS$_2$**). Therefore, we conclude that the bridging carbene **E** is not formed in practice, and this is likely a factor contributing to the improved catalytic activity of [Co(MeTAA)]. In contrast, for [Co(TPP)] the bridging carbene **E"** has a lower free energy (−4.5 kcal mol^{-1}) than the carbene radical **B"** (−3.4 kcal mol^{-1}).

The second step, as seen in Fig. 7, is the addition of methyl acrylate to the carbene radical **B**. This addition has a lower barrier (**TS$_{2\text{-trans}}$** = +6.7 kcal mol^{-1}) when attacking *trans* to the ethyl ester attached to the carbene than for **TS$_{2\text{-cis}}$** = +11.1 kcal mol^{-1} for *cis* attack. This difference (4.4 kcal mol^{-1}) is in line with the experimental data showing a high *trans:cis* ratio between the different cyclopropane diastereoisomers of 97:3 [11]. Therefore, computations also favor the pathway leading to the formation of the trans-isomer.

The last step is the cyclization of γ-radical **C** to form cyclopropane. The transition state, **TS$_{3\text{-CoMeTAA}}$** = +3.6 kcal mol^{-1}, is similar to the corresponding step in the mechanism of the [Co(TPP)]-catalyzed cyclopropanation reaction, **TS$_{3\text{-CoTPP}}$** = +3.1 kcal mol^{-1} (Fig. 9). Compared with the other reaction steps in the catalytic cycle, it is the lowest barrier of the entire energy diagram, and thus should not influence the overall kinetics of the reaction.

Therefore, looking at all free energy barriers, the DFT calculations predict the [Co(MeTAA)]-catalyzed reaction to be first-order in [EDA] and [catalyst] and zero-order in [methyl acrylate]. Nitrogen release and carbene radical formation should be the rate-determining step, with a transition state barrier of $\Delta G^{\ddagger}_{298K}$ = +14.5 kcal mol^{-1}. When this mechanism is compared with the one using [Co(TPP)] as a catalyst, it can be observed that all steps are similar, and the main intermediates present a similar radical character. However, the relative energies of the involved species, including the transition states, vary significantly. Noteworthy is the high barrier of the nitrogen release step with **TS$_{1\text{-CoTPP}}$** = +19.5 kcal mol^{-1}. The difference of +5.0 kcal mol^{-1} between the transition states of the rate-determining step can explain the longer reaction times noticed during experiments using [Co(TPP)], in contrast to [Co(MeTAA)] (see Section 2, Fig. 5). It should further be noted here that the dispersion-corrected DFT calculations of the [Co(TPP)]-catalyzed

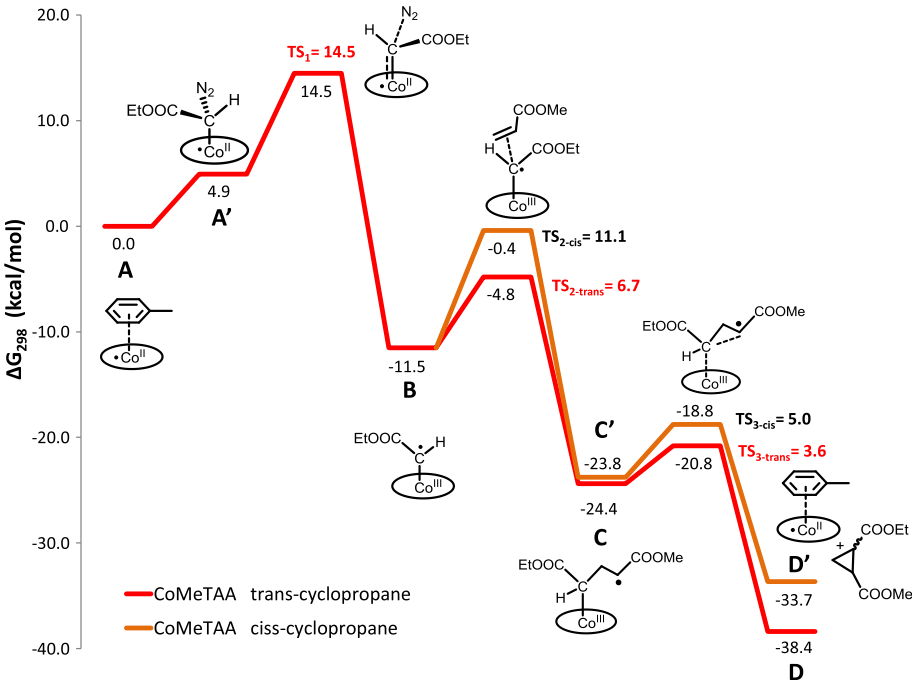

Fig. 7. Energy diagram of the [Co(MeTAA)]-catalyzed cyclopropanation of methyl acrylate with ethyl diazoacetate. All energies are relative to **A** (transition state barriers relative to the preceding intermediate).

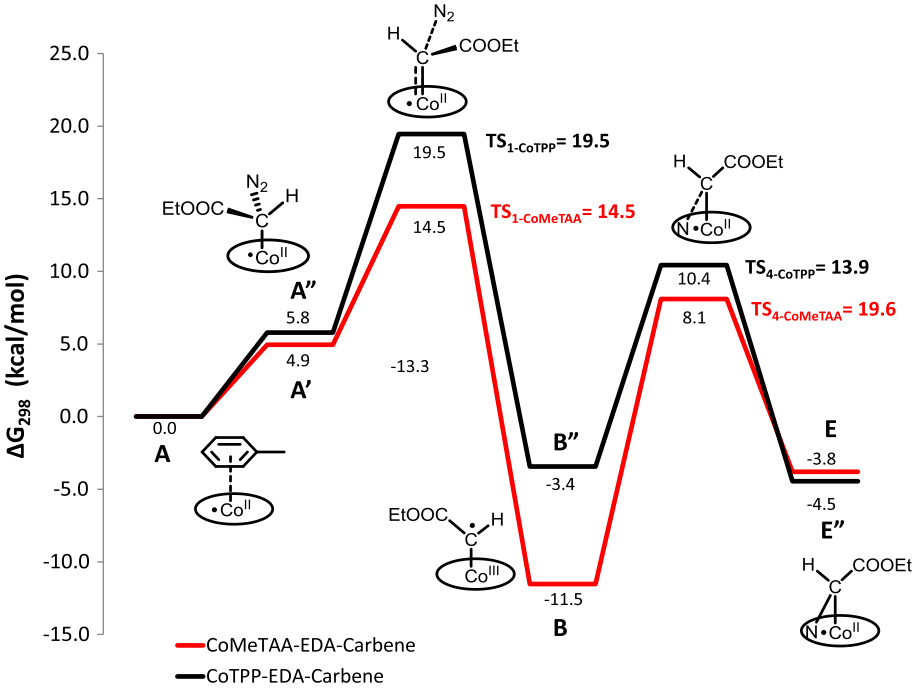

Fig. 8. Energy diagram of the activation of EDA with [Co(MeTAA)] and [Co(TPP)] and generation of carbene radicals or bridging carbenes. All energies are relative to **A** (transition state barriers relative to the preceding intermediate).

steps reported here differ slightly from previously reported calculations performed in our group [10], in the sense that addition of the carbene radical **B** to the acrylate substrate is computed to have a lower barrier than formation of **B** via **TS1** when Grimme's version 3 dispersion corrections are used, while the computed barriers for these process are very similar in calculations without dispersion corrections.

Thus, as shown above for [Co(MeTAA)], DFT therefore predicts first-order kinetics in [EDA] and [catalyst], but zero-order kinetics in [methyl acrylate] under catalytically relevant reaction conditions for [Co(TPP)]. Only at (very) low acrylate concentrations should the reaction become first-order in [methyl acrylate]. This seems to correlate directly with the experimentally determined bell-shaped rate dependence on the olefin concentration detected

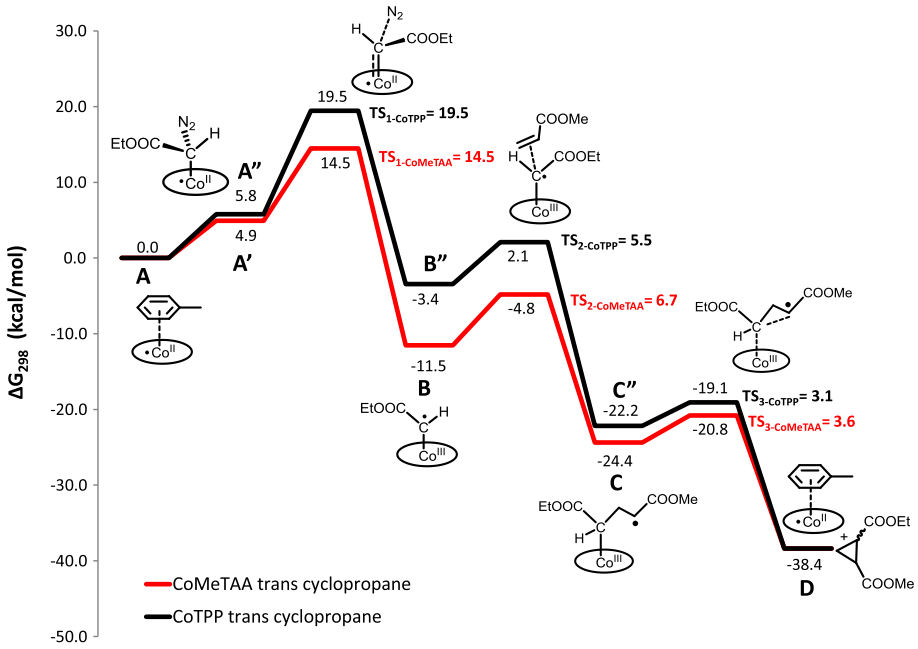

Fig. 9. Energy diagram comparison of the [Co(MeTAA)]- and [Co(TPP)]-catalyzed cyclopropanation of methyl acrylate with ethyl diazoacetate. All energies are relative to **A** (transition state barriers relative to the preceding intermediate).

at low olefin concentrations in kinetic studies of styrene cyclopropanation with [Co(TPP)], as reported by Cenini and Gallo [5].

Initial experimental efforts to shine more light on the mechanism of the [Co(MeTAA)]-catalyzed reactions focused on detecting reaction intermediates using spin trapping combined with EPR spectroscopy and high-resolution mass spectrometry. Only one previous study has been performed in which "carbene radicals" were directly detected by EPR, and that was the reaction between EDA and [Co(3,5-Di^{t}Bu-ChenPhyrin)], a bulky porphyrin ligand with stabilizing hydrogen-bond donor motifs. However, with other, simpler cobalt(II) porphyrin complexes such as [Co(TPP)], similar carbene radical species could not be detected with EPR spectroscopy. Reactions with EDA resulted in EPR silent solutions in the temperature range between 5 and 70 K, implying either EPR silence of the key carbene intermediate (e.g., due to rapid relaxation effects) or rapid conversion of the "carbene radicals" to diamagnetic species (e.g., [Co^{III}(TPP)-(CH_2COOEt)]; see Ref. [5]) under these conditions.

The [Co(MeTAA)] complex behaves in a manner similar to [Co(TPP)], and also produces EPR silent solutions (at 20 K) upon reaction with EDA (or EDA and methyl acrylate). However, high-resolution MS obtained via cold spray ionization at −40 °C (Fig. 10) revealed the presence of [Co(MeTAA)(CHCOOEt)]$^+$, i.e., 1e-oxidized species **B** (m/z = 487.1536). Detection of these species is in agreement with the DFT-computed mechanism. A species with mass m/z = 573.1864, corresponding to [Co(MeTAA)(CHCOOEt)(MeAcrylate)]$^+$, was also detected. While this could point to 1e-oxidized species **C** or **F** (Fig. 10), it could also be the cyclopropane adduct (e.g., bound with its ester moiety) of 1e-oxidized [Co(MeTAA)] species **A**.

Spin trapping can be used as an indirect method to detect radical species by EPR [22]. It usually involves a nitrone as the spin trap that reacts with a reactive, short-lived free radical, forming a nitroxide-based persistent radical that can easily be detected by EPR. Most typically, *N-tert*-butyl-α-phenylnitrone (PBN) or 5,5-dimethyl-pyrroline N-oxide (DMPO) is the spin-trapping reagent used in this approach (Fig. 11). They easily react with free radicals in the α-position, generating persistent nitroxide radicals that are

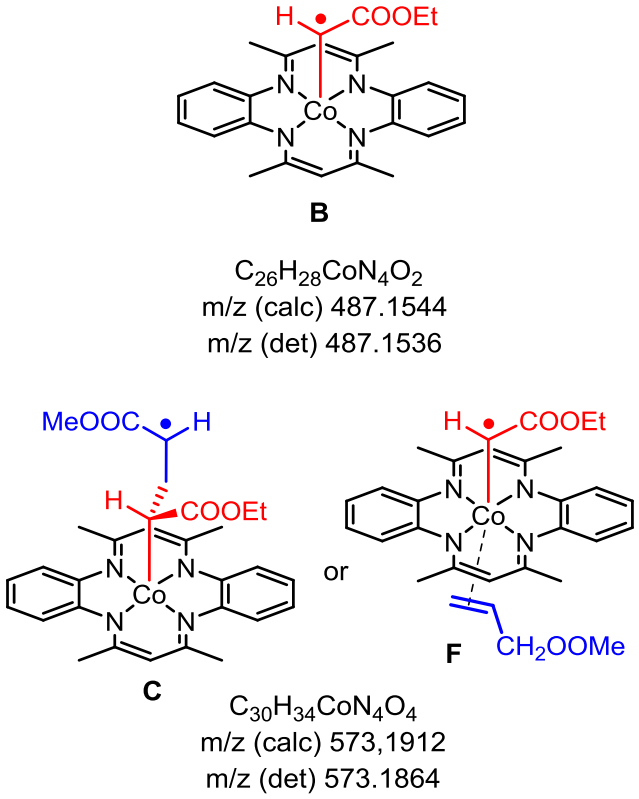

Fig. 10. Proposed intermediates of the [Co(MeTAA)]-catalyzed cyclopropanation of methyl acrylate with ethyl diazoacetate, detected using CSI-HRMS at −40 °C.

stable for days and can be detected by EPR at room temperature (Fig. 11). By looking at the EPR profile, some information can be inferred about the trapped radical. The most revealing characteristics are the *g*-value and the hyperfine couplings.

Upon recording EPR spectra during the [Co(MeTAA)]-catalyzed cyclopropanation reaction, adding PBN or DMPO as the spin traps,

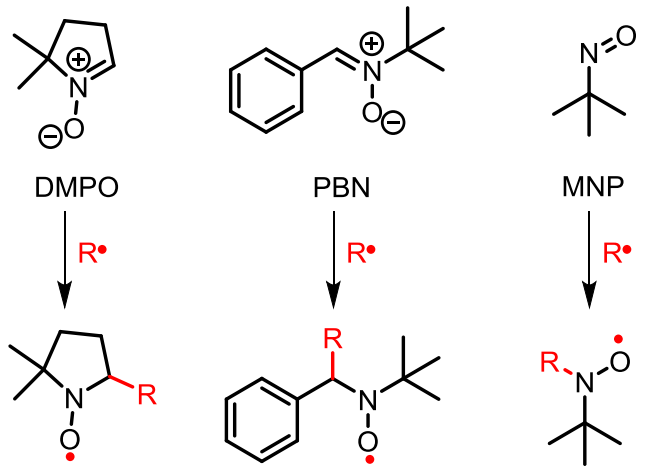

Fig. 11. Formation of persistent radicals using the most common trapping agents.

we observed an isotropic hyperfine splitting pattern characteristic for a trapped carbon-centered radical (Fig. 12) [23]. The EPR signal of the PBN-trapped species is strong and clean, much more intense than the background signal measured by recording the spectrum under identical conditions, but leaving out the EDA reagent. The signal obtained from the DMPO adduct is not as clean, but can still be characterized as a trapped carbon radical. Both spin adducts are used as complementary evidence, each characteristic of trapping a carbon-centered radical. While these experiments do not allow us to distinguish between different carbon radicals, we assume it is the carbene radical complex **B** (Scheme 1) that is trapped in these experiments (Fig. 12). We cannot fully exclude the possibility that it is species **C** that is trapped in these experiments, though.

We further decided to investigate the kinetic profile of the [Co(MeTAA)]-catalyzed cyclopropanation reaction. However, before starting our kinetic studies, we first examined the influence of some experimental conditions on the outcome of the reaction, such as the order of reagent addition, variations in concentration, or determining the lower limit of catalyst loading. If EDA is added to the reaction mixture after methyl acrylate, the reaction proceeds normally. However, if this order is reversed, the reaction does not take place at all, as is clear from the constant nitrogen pressure, showing no increase. Moreover, the byproducts of the 1,3-dipolar addition products, formed in the uncatalyzed reaction between EDA and methyl acrylate, are observed in the ^{1}H NMR spectrum (Scheme 2). This can be explained by catalyst deactivation caused by the reactive carbene intermediate formed from EDA in the absence of the acrylate substrate, which will most likely abstract a hydrogen atom from the reaction medium or the EDA substrate to produce the deactivated Co^{III}-CH_2COOEt species (in the absence of methyl acrylate). This is in agreement with the formation of EPR-silent solutions upon reaction of [Co(MeTAA)] with EDA (vide supra). If only ethyl diazoacetate is added to the reaction mixture to see if diethyl fumarate is formed, carbene dimerization (as observed for many other catalysts) is not observed for [Co(MeTAA)], again indicating rapid deactivation to Co^{III}-CH_2COOEt species under these conditions.

The design of the actual kinetic experiments follows Blackmond's RPKA method [12] to measure the reaction progress in time (release of dinitrogen vs. time). Release of dinitrogen is directly proportional to EDA consumption over time. A proper theoretical model of the system is needed to interpret the results. Here we used the following kinetic model. The general form of the rate equation for our reaction is

$$\text{rate} = k_r \cdot [\text{EDA}]^x [\text{MeAcryl}]^y [\text{cat}]^z.$$

However, looking at the DFT mechanism, we assume $x = 1$, $y = 0$, and $z = 1$, which should be confirmed experimentally. Therefore,

$$\text{rate} = k_r \cdot [\text{EDA}] \cdot [\text{cat}].$$

In a reaction where there is no catalyst deactivation, $[\text{cat}] = [\text{cat}]_0$

However, preliminary results of the kinetic experiments indicate catalyst deactivation. Therefore, we assume a first-order cata-

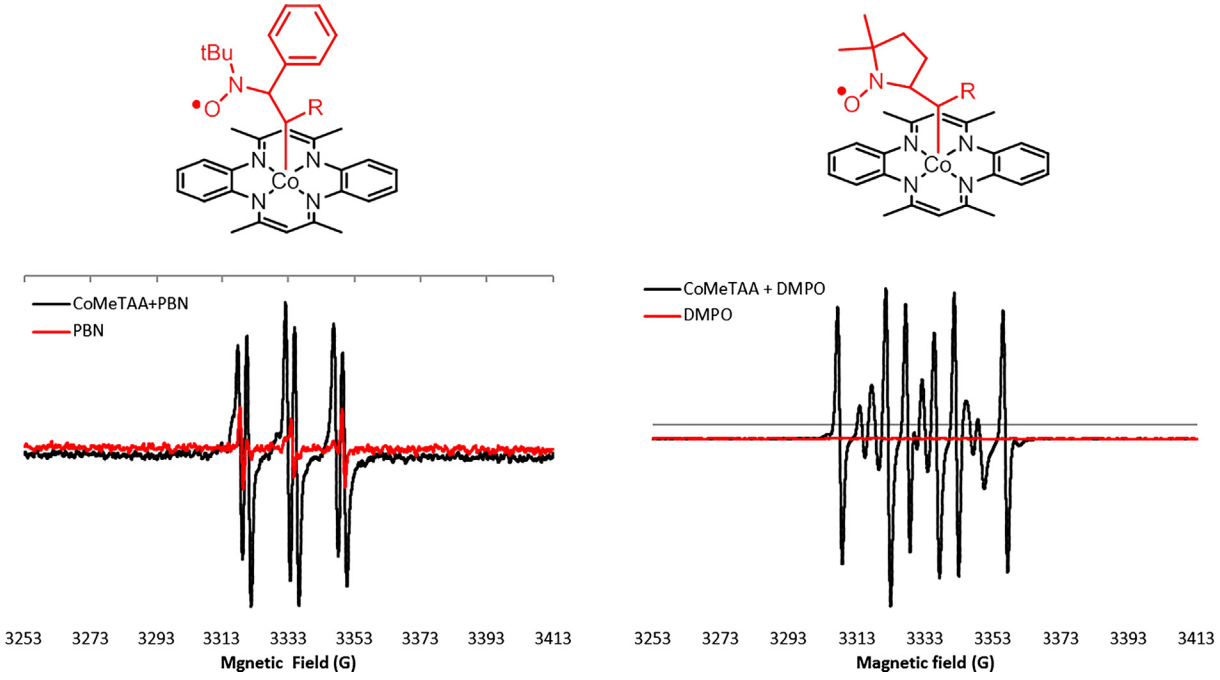

Fig. 12. Isotropic X-band EPR spectrum of the PBN (left)- and DMPO (right)-trapped carbon-centered radicals (T = 298 K; microwave frequency: 9.36607 GHz; power: 6.33 mW; modulation amplitude: 1.0 G).

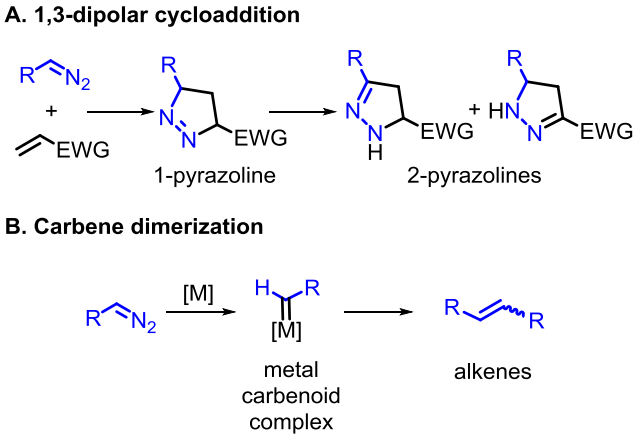

Scheme 2. (A) 1,3-Dipolar cycloaddition between a diazo compound and an electron-deficient alkene, observed upon addition of EDA before methyl acrylate. (B) Diazo compound dimerization toward alkenes via metal carbenoids [24] is not observed using [Co(MeTAA)].

lyst deactivation process, which should also be confirmed experimentally:

$$\text{rate}_{\text{deact}} = k_d \cdot [\text{cat}],$$

$$\frac{d[\text{cat}]}{dt} = -k_d \cdot [\text{cat}],$$

$$\frac{d[\text{cat}]}{[\text{cat}]} = -k_d \cdot dt,$$

$$\int_{[\text{cat}]_0}^{[\text{cat}]} \frac{1}{[\text{cat}]} d[\text{cat}] = \int_0^t -k_d dt,$$

$$\ln[\text{cat}] - \ln[\text{cat}]_0 = -k_d \cdot t,$$

$$[\text{cat}] = [\text{cat}]_0 \cdot e^{-k_d \cdot t}. \quad (1)$$

When the above-mentioned reaction steps are combined in the kinetic rate equation, the integrated form of the rate equation becomes

$$\text{rate} = k_r \cdot [\text{EDA}] \cdot [\text{cat}],$$

$$\frac{d[\text{EDA}]}{dt} = -k_r \cdot [\text{EDA}] \cdot [\text{cat}]_0 \cdot e^{-k_d \cdot t},$$

$$\frac{d[\text{EDA}]}{[\text{EDA}]} = -k_r \cdot [\text{cat}]_0 \cdot e^{-k_d \cdot t} dt,$$

$$\int_{[\text{EDA}]_0}^{[\text{EDA}]} \frac{1}{[\text{EDA}]} d[\text{EDA}] = \int_0^t -k_r \cdot [\text{cat}]_0 \cdot e^{-k_d \cdot t} dt,$$

$$\ln[\text{EDA}] - \ln[\text{EDA}]_0 = -k_r \cdot [\text{cat}]_0 \cdot \left(\frac{-e^{(-k_d \cdot t)}}{k_d} + \frac{1}{k_d} \right),$$

$$[\text{EDA}] = [\text{EDA}]_0 \cdot e^{\left(\frac{-k_r \cdot [\text{cat}]_0 \cdot \left(1 - e^{-k_d \cdot t}\right)}{k_d} \right)}, \quad (2)$$

where

$$k_r = \frac{k_B T}{h} e^{\frac{\Delta G_r^{\ddagger}}{RT}} \text{L} \cdot \text{mol}^{-1} \cdot \text{min}^{-1},$$

$$k_d = \frac{k_B T}{h} e^{\frac{\Delta G_d^{\ddagger}}{RT}} \text{min}^{-1},$$

$$\Delta G^{\ddagger} = \Delta H^{\ddagger} - T\Delta S^{\ddagger},$$

where k_r = reaction rate constant ($\text{L} \cdot \text{mol}^{-1} \cdot \text{min}^{-1}$), k_d = catalyst deactivation rate constant (min^{-1}), k_B = Boltzmann constant $\left(4.970334 \times 10^{-20} \text{m}^2 \cdot \text{kg} \cdot \text{min}^{-2} \cdot \text{K}^{-1}\right)$, t = reaction time (min), T = absolute temperature (K), h = Planck's constant $\left(3.975642 \times 10^{-32} \text{m}^2 \cdot \text{kg} \cdot \text{min}^{-1}\right)$, $\Delta G^{\ddagger}$ = Gibbs energy of activation ($\text{kcal} \cdot \text{mol}^{-1}$), $\Delta H^{\ddagger}$ = enthalpy of activation ($\text{kcal} \cdot \text{mol}^{-1}$), $\Delta S^{\ddagger}$ = entropy of activation ($\text{kcal} \cdot \text{mol}^{-1}$), and R = gas constant ($1.987 \times 10^{-3} \text{kcal} \cdot \text{mol}^{-1} \cdot \text{K}^{-1}$).

We fitted all experimental kinetics to the above rate equations. We started the experimental kinetic studies by measuring the reaction progress [EDA], consumption versus time (Fig. 13), at three different catalyst loadings, considering equal substrate concentrations. Using the integrated form of the proposed rate equation (Eq. (2)), excellent fits of the experimental data were achieved. All experiments having different initial catalyst loadings, but performed at the same temperature (283 K), afforded k_r = 85.0 L mol^{-1} min^{-1} and k_d = 0.18 min^{-1}. Obtaining the same rate constants for different experiments performed at the same temperature is a strong indication that the proposed rate equation (Eq. (2)) is correct. However, we nonetheless decided to apply Blackmond's methodology by plotting several types of graphs such as [substrate] vs. time or rate vs. [substrate], in which the kinetic experiments are discussed in detail. This method uses a more graphical approach, which is perhaps more intuitive to experimental chemists.

By conducting experiments at different initial catalyst concentrations, it is possible to determine the order of the reaction in [catalyst]. If the reaction is first-order in [catalyst], which it is usually the case for homogeneous catalysts, the rate dependence on the catalyst concentration is linear, and therefore the reaction rate is doubled when the catalyst concentration is doubled. An essential factor that needs to be taken into account in these experiments is that the active [Co(MeTAA) catalyst concentration does not remain constant throughout the reaction, but decays following a first-order deactivation process. Catalyst decay is, however, substantially slower than the catalytic reaction. Importantly, if this deactivation process is not taken into consideration the kinetic data cannot be fitted properly.

From Figs. 13 and 14 it can easily be observed that the reaction rate increases with the increase in catalyst concentration. However, to determine the reaction order in [Co(MeTAA)] the turnover frequency (TOF) has to be plotted versus [EDA] (Fig. 15). If the curves of different experiments overlap, the reaction is first-order in [catalyst] [12]. An explanation for this can be found in the TOF definition, where TOF = rate/[catalyst]. Doubling both rate and [catalyst] leads to the same TOF for different experiments at the same [EDA], therefore implying curve overlap. If the reaction has a different order than one, then the curves will not overlap. In Fig. 15, the plot of the TOF versus [EDA] at 2.7 mol.%, 2.0 mol.%,

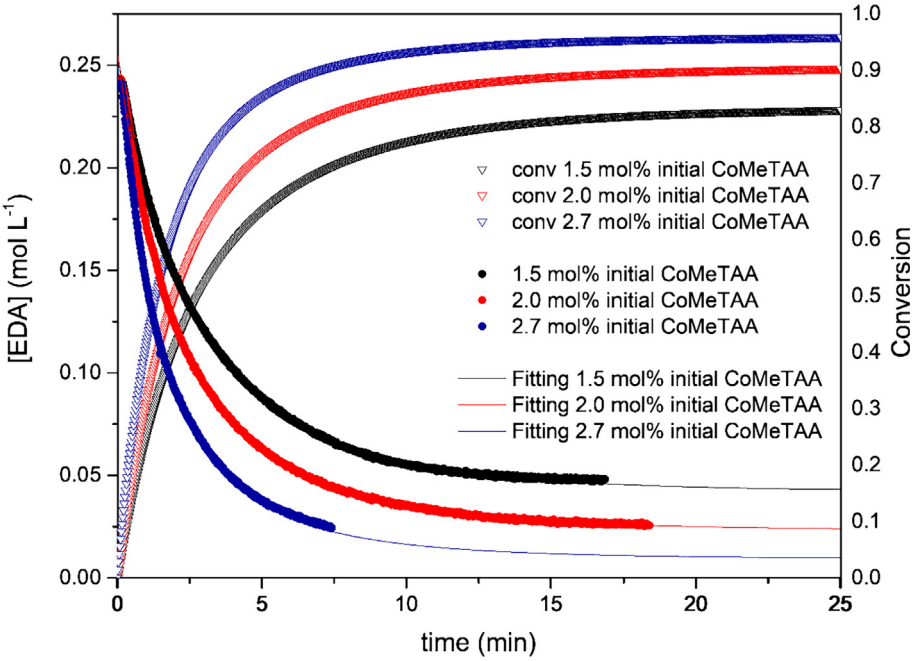

Fig. 13. [EDA] vs. time and conversion vs. time for experiments at different catalyst loadings.

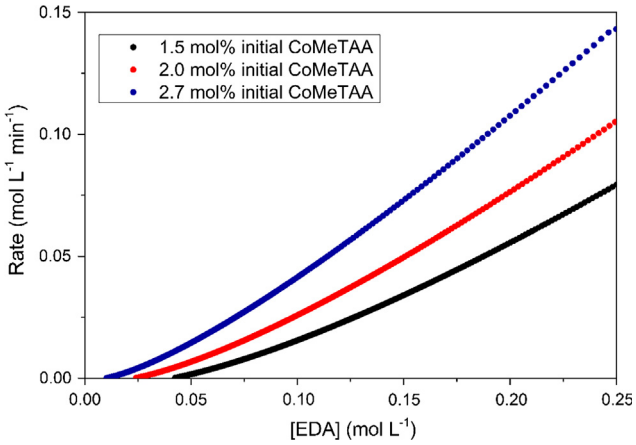

Fig. 14. Rate versus [EDA] for experiments at different catalyst loadings.

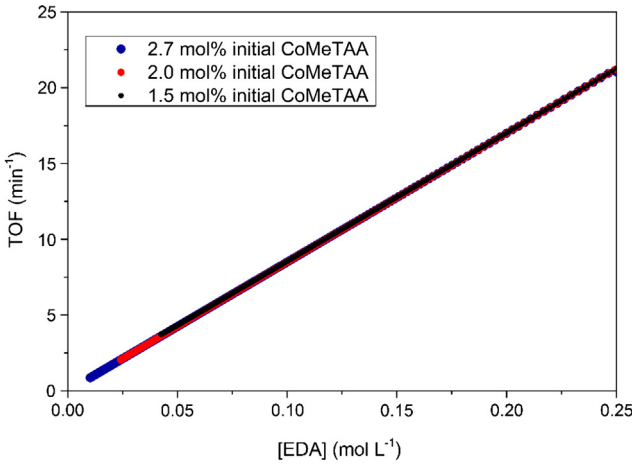

Fig. 15. TOF versus [EDA] for experiments at different catalyst loadings.

and 1.5 mol.% [Co(MeTAA)] do overlap, therefore showing first-order kinetics in [catalyst].

To confirm that catalyst deactivation indeed occurs during the catalytic experiments at lower catalyst concentrations, catalytic reactions were explored using different substrate concentrations but keeping the difference between the concentration of methyl acrylate and EDA constant. These are so-called "same excess" experiments ([excess] = [MeAcrylate] – [EDA]). The kinetic data extracted from these experiments can be used to distinguish between catalyst deactivation and product inhibition during catalysis.

Three of such "same excess" experiments are shown in Fig. 16. Two of them are designed to have lower initial substrate concentrations, chosen so that the initial substrate concentrations of these experiments are equal to the substrate concentrations at 25% and 50% conversion of the standard reaction, respectively (see Section 2). These reactions thus simulate the standard reaction at 25% and 50% conversion, but starting with a fresh batch of catalyst and in the absence of product, which provides information about both catalyst deactivation and product inhibition. In the absence of catalyst deactivation or product inhibition, the rates should be the same under all conditions and substrate concentrations screened, and hence the conversion vs. time plots should overlap. This is not the case, as seen in Fig. 16. The same excess experiments simulating 25% and 50% conversion of the standard reaction but starting with fresh catalyst and in the absence of product are clearly faster.

The occurrence of catalyst deactivation and/or product inhibition processes is most clearly visualized by the nonoverlapping plots of reaction rate vs. [EDA] (Fig. 17). To distinguish between catalyst deactivation and product inhibition, an additional kinetic experiment was performed adding the cyclopropane product to the reaction mixture (Fig. 17). Using a lower initial substrate concentration, 50% of the standard reaction, fresh catalyst, and adding the cyclopropane product in the same concentration as formed under the standard reaction conditions at 50% conversion, the rate plots overlap nicely, indicating no product inhibition. However, it is clear that the reactions starting with fresh catalyst (magenta and purple curves in Fig. 17) are always significantly faster than

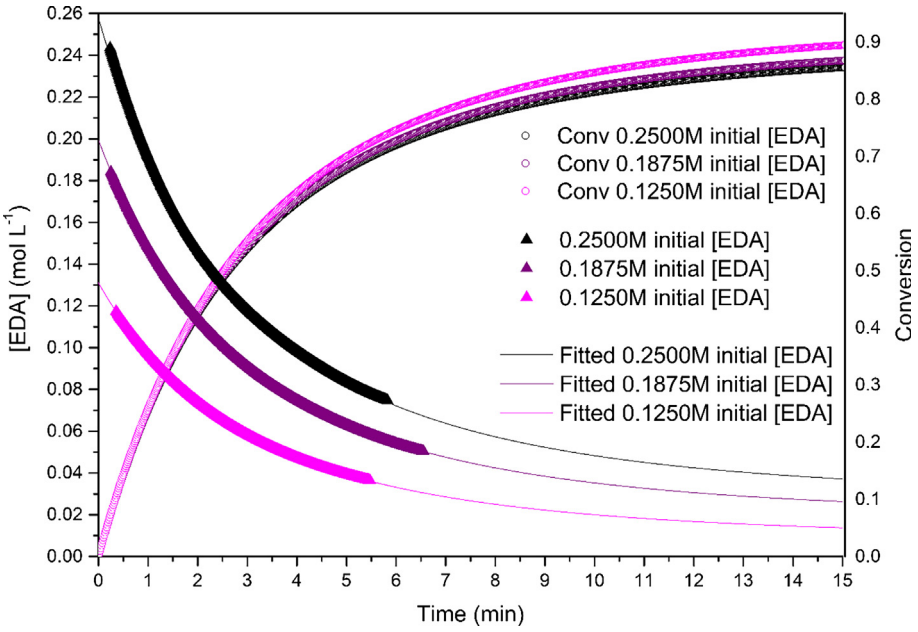

Fig. 16. [EDA] vs. time and conversion vs. time for "same excess" experiments.

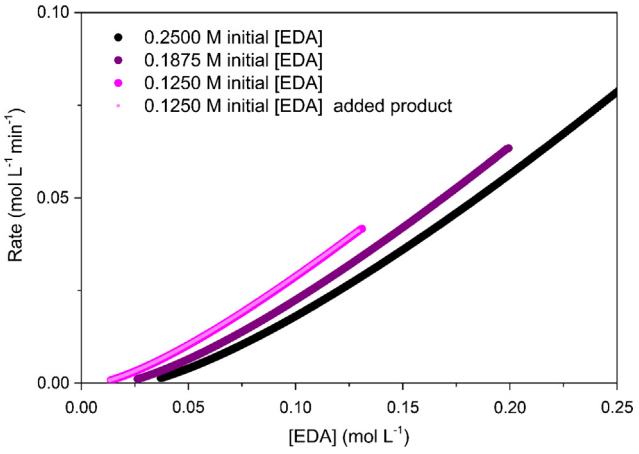

Fig. 17. Rate versus [EDA] plots of the "same excess" experiments.

those after 50% conversion under otherwise identical conditions at the same concentrations of EDA. This clearly points to gradual catalyst deactivation under the applied reaction conditions, in line with the proposed first-order deactivation rate equation (Eq. (1)).

The [substrate] reaction orders were determined by conducting experiments at "different excess" concentrations of methyl acrylate. If the reaction is zero-order in [methyl acrylate], the concentration of methyl acrylate will have no effect on the reaction rate. Fig. 18 shows a plot of the reaction conversion over time as well as of the consumption of [EDA] over time, for different excesses of methyl acrylate. There is a clear overlap of the curves, with a slight misalignment when both reactions reach conversion >70%. To see the overlap better, the reaction rate versus [EDA] is plotted in Fig. 19, and it indeed shows that the two curves overlap. The reaction is therefore zero-order in [methyl acrylate] under the actually applied reaction conditions. To determine the reaction order in [EDA], the plot of the TOF (rate/[catalyst]) vs. the EDA concentration should be analyzed. By looking at the graph, it can be seen that the plot is a straight line, which implies first-order kinetics in [EDA].

After in-depth analysis of all the kinetic data and fitting of the experimental data with the proposed model, we arrive at the following rate equations for the [Co(MeTAA)]-catalyzed cyclopropanation of methyl acrylate with EDA,

$$\text{rate} = k_r \cdot [\text{EDA}] \cdot [\text{cat}] \tag{3}$$

$$\text{where } [\text{cat}] = [\text{cat}]_0 \cdot e^{-k_d \cdot t}$$

and $k_r = 85.0$ L mol^{-1} min^{-1} and $k_d = 0.18$ min^{-1} (both averaged over many experiments) measured at 283 K. These rate constants are temperature-dependent; thus, we decided to perform the kinetic experiments at three different temperatures (273, 278, and 283 K) in order to derive both the enthalpy and entropy of activation for direct comparison with the DFT calculations. Fig. 20 shows, as expected, that the reaction is slower when the reaction is performed at lower temperatures.

After the experimental data are fitted using Eq. (2), the reaction rate constants can be obtained at the three different temperatures. Therefore, at 273 K, $k_{273} = 46$ L mol^{-1} min^{-1} was obtained, at 278 K, $k_{278} = 64$ L mol^{-1} min^{-1}, and at 283 K, $k_{283} = 85$ L mol^{-1} min^{-1}. The Eyring equation can be used to understand the influence of temperature over the reaction rate, as it shows the relation between k and T, from which the Gibbs free energy of activation can be derived:

$$k_r = \frac{k_B T}{h} e^{\frac{\Delta G_r^{\ddagger}}{RT}}. \tag{4}$$

The linear form of the Eyring–Polanyi equation is most useful for plotting linear graphs, and can be expressed as

$$\ln\frac{k_r}{T} = \frac{-\Delta H^{\ddagger}}{R} \cdot \frac{1}{T} + \ln\frac{k_B}{h} + \frac{\Delta S^{\ddagger}}{R}. \tag{5}$$

By performing the reaction at different temperatures, and plotting $\ln\frac{k_r}{T}$ vs. $\frac{1}{T}$, a straight line is expected from which both $\Delta H^{\ddagger}$ and $\Delta S^{\ddagger}$ can be derived. The thus-obtained experimental values for enthalpy and entropy can then be compared with the DFT-calculated values of the rate-determining step. Fig. 21 presents a good fitting of the reaction rates at three different temperatures.

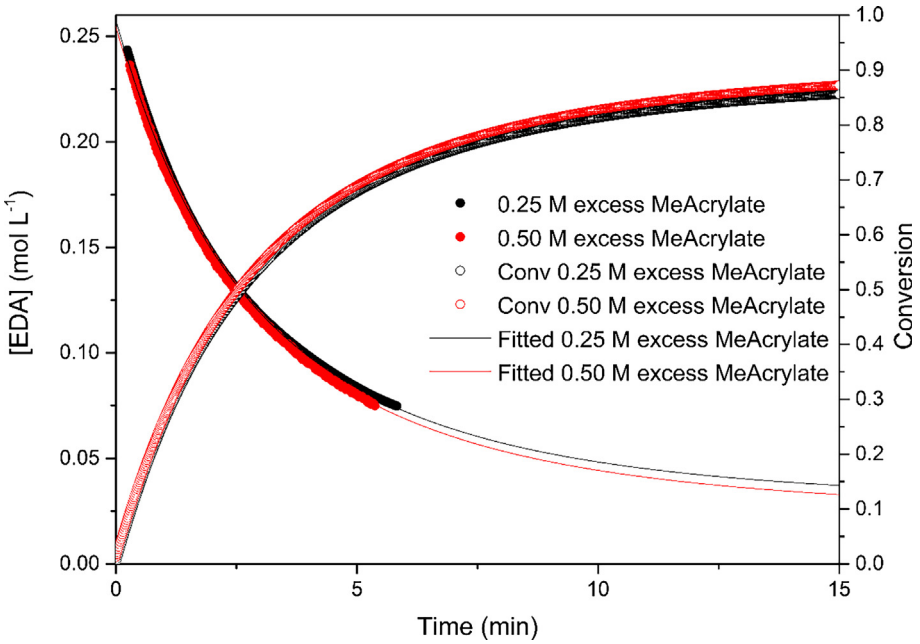

Fig. 18. [EDA] vs. time and conversion vs. time for "different excess" experiments.

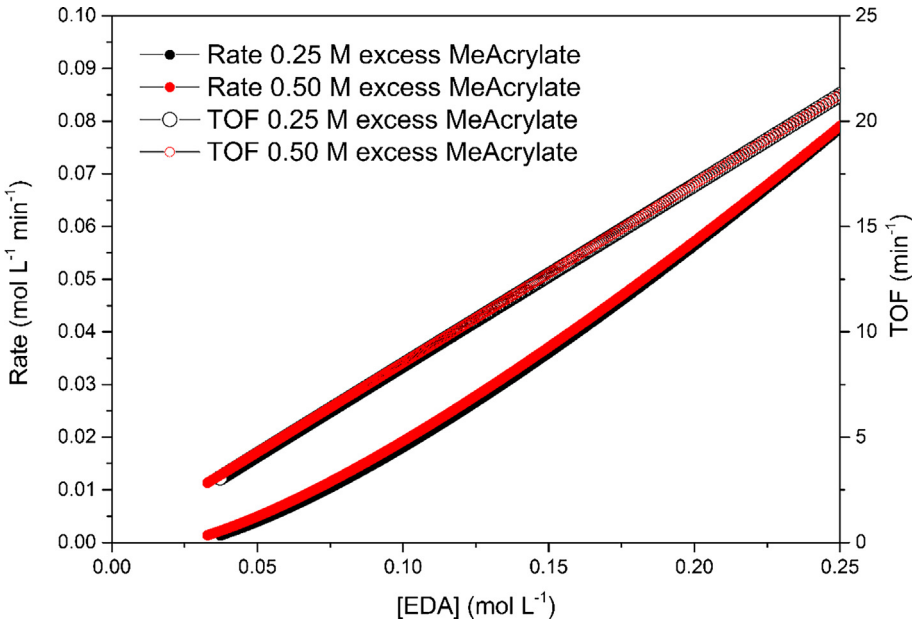

Fig. 19. Rate vs [EDA] and TOF vs [EDA] plots for "same excess" experiments.

From the fitting equations, we obtained $\Delta H^{\ddagger}$ = +8.89 kcal mol^{-1} and $\Delta S^{\ddagger}$ = −26.4 cal mol^{-1} K^{-1}, which translates ($\Delta G^{\ddagger} = \Delta H^{\ddagger} - T\Delta S^{\ddagger}$) to a free energy activation barrier of $\Delta G^{\ddagger}_{298}$ = +16.8 kcal mol^{-1} at 298 K. The substantial negative activation entropy term points to an ordered transition state, as expected for the proposed associative process (from **A** to the rate-limiting transition state **TS1**; see Scheme 1, Fig. 7).

The experimental free energy activation barrier $\Delta G^{\ddagger}_{298}$(exp) = +16.8 kcal mol^{-1} is in good qualitative agreement with the calculated one $\Delta G^{\ddagger}_{298}$(calc) = +14.5. The small difference of 2.3 kcal mol^{-1} is likely, at least in part, due to some (experimental and computational) errors in the activation entropy term (Table 2).

Overall, the experimental and DFT-calculated activation parameters are in good agreement. The most reliable parameters (both experimentally and computationally) are the activation enthalpies. The DFT-calculated activation enthalpy ($\Delta H^{\ddagger}_{calc}$ = +7.8 kcal mol^{-1}) is in excellent agreement with the experimental one ($\Delta H^{\ddagger}_{exp}$ = +8.9 kcal mol^{-1}), thus giving strong support to the proposed mechanism shown in Scheme 1.

4. Summary and conclusions

In summary, a detailed mechanistic study of the cobalt(II) tetra methyl–dibenzotetraaza[14]annulene [Co(MeTAA)]-catalyzed cyclopropanation of methyl acrylate with ethyl diazoacetate

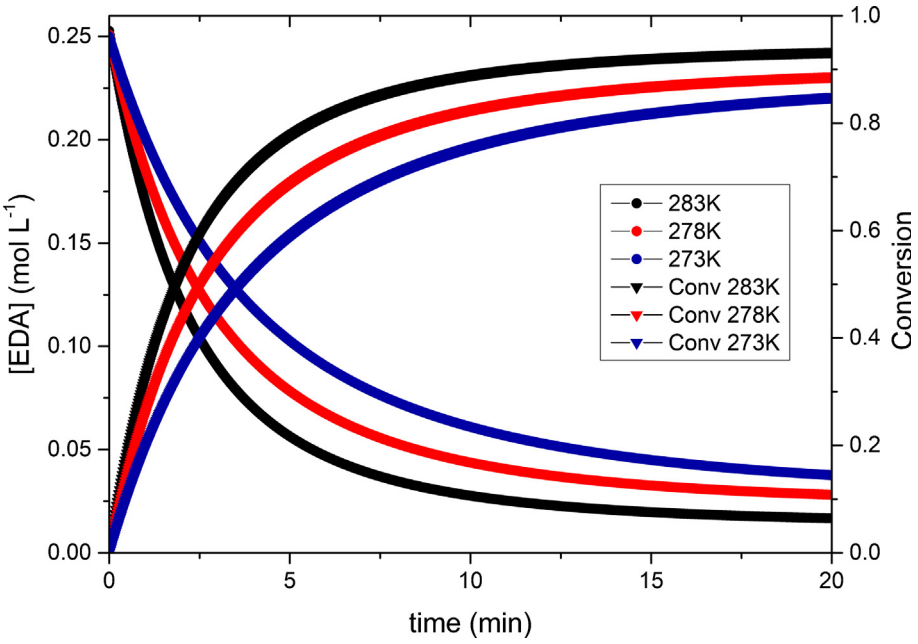

Fig. 20. [EDA] vs. time and conversion vs. time at different temperatures.

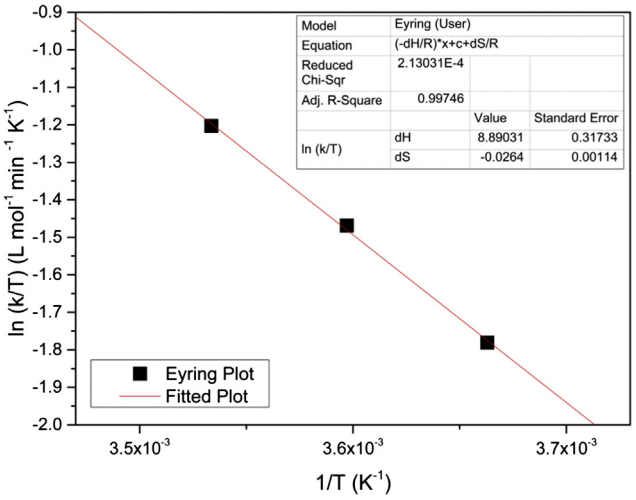

Fig. 21. Eyring linear plot ($ln\frac{k_r}{T}$ vs. $\frac{1}{T}$).

Table 2
Comparison of experimental and DFT-calculated activation parameters of the [Co(MeTAA)]-catalyzed cyclopropanation reaction of methyl acrylate with EDA.

	$\Delta G^{\ddagger}_{298}$ [a]	$\Delta H^{\ddagger}_{298}$ [a]	$\Delta S^{\ddagger}_{298}$ [b]
Experiment	+16.8 (±0.3)	+8.9 (±0.3)	−26 (±1.1)
DFT	+14.5	+7.8	−22

[a] Activation energies in kcal mol^{-1}.
[b] Activation entropies in e.u. (cal mol^{-1} K^{-1}).

(EDA) has been performed. The DFT study revealed that the overall free energy barriers of the [Co(MeTAA)]-catalyzed reaction are significantly lower than those for the [Co(TPP)]-catalyzed process. In good agreement, experimental kinetic studies revealed substantially faster reactions for the [Co(MeTAA)]-catalyzed reactions. Cobalt(III)-carbene radicals were demonstrated to be present as key intermediates in the reaction and were detected using HR-MS and EPR spin-trapping experiments. Real-time reaction monitoring allowed us to use RPKA to analyze the experimental data. These studies revealed that the reaction is first-order in both [catalyst] and [EDA] and zero-order in [methyl acrylate], in excellent agreement with the DFT-calculated mechanism. Furthermore, a first-order catalyst deactivation process was detected, which is much slower than the catalytic reaction steps, but does lead to detectable catalyst degradation during catalysis. The exact nature of this process needs to be further investigated in future studies. The DFT calculated activation parameters of the reaction ($\Delta G^{\ddagger}$, $\Delta H^{\ddagger}$, and $\Delta S^{\ddagger}$) are in agreement with the experimental values, thus providing strong support for the proposed metalloradical mechanism.

Acknowledgments

We thank Ed Zuidinga for MS measurements and Jan Meine Ernsting for NMR advice. Dr. W.I. Dzik is acknowledged for helpful discussions. Financial support from the Netherlands Organization for Scientific Research (NWO-CW VICI project 016.122.613) and the University of Amsterdam (Research Priority Area Sustainable Chemistry) is gratefully acknowledged.

Appendix A. Supplementary material

Supporting information containing details of the computational studies and a zip file containing the Cartesian coordinates of the optimized geometries (xyz format) are available as separate files. Supplementary data associated with this article can be found, in the online version, at https://doi.org/10.1016/j.jcat.2018.02.013.

References

[1] (a) M.P. Doyle, D.C. Forbes, Chem. Rev. 98 (1998) 911–935;
(b) W. Kirmse, Angew. Chem. Int. Ed. 42 (2003) 1088–1093;
(c) H.M.L. Davies, S.J. Hedley, Chem. Soc. Rev. 36 (2007) 1109–1119;
(d) A.G.H. Wee, Curr. Org. Synth. 3 (2006) 499–555.
[2] (a) A. Nakamura, A. Konishi, Y. Tatsuno, S. Otsuka, J. Am. Chem. Soc. 100 (1978) 3443–3448;
(b) A. Nakamura, A. Konishi, R. Tsujitani, M. Kudo, S. Otsuka, J. Am. Chem. Soc. 100 (1978) 3449–3461.
[3] (a) T. Niimi, T. Uchida, R. Irie, T. Katsuki, Tetrahedron Lett. 41 (2000) 3647–3651;
(b) T. Niimi, T. Uchida, R. Irie, T. Katsuki, Adv. Synth. Catal. 33 (2001) 79–88.

[4] (a) L. Huang, Y. Chen, G.-Y. Gao, X.P. Zhang, J. Org. Chem. 68 (2003) 8179–8184;
(b) Y. Chen, K.B. Fields, X.P. Zhang, J. Am. Chem. Soc. 126 (2004) 14718–14719;
(c) Y. Chen, X.P. Zhang, J. Org. Chem. 72 (2007) 5931–5934;
(d) Y. Chen, J.V. Ruppel, X.P. Zhang, J. Am. Chem. Soc. 129 (2007) 12074–12075;
(e) S. Zhu, J.V. Ruppel, H. Lu, L. Wojtas, X.P. Zhang, J. Am. Chem. Soc. 130 (2008) 5042–5043;
(f) S. Zhu, J.A. Perman, X.P. Zhang, Angew. Chem. Int. Ed. 7 (2008) 8460–8463;
(g) J.V. Ruppel, T.J. Gauthier, N.L. Snyder, J.A. Perman, X.P. Zhang, Org. Lett. 11 (2009) 2273–2276.
[5] A. Penoni, R. Wanke, S. Tollari, E. Gallo, D. Musella, F. Ragaini, F. Demartin, S. Cenini, Eur. J. Inorg. Chem. (2003) 1452–1460.
[6] A. Caselli, M.G. Buonomenna, F. de Baldironi, L. Laera, S. Fantauzzi, F. Ragaini, E. Gallo, G. Golemme, S. Cenini, E. Drioli, J. Mol. Catal. A Chem. 317 (2010) 72–80.
[7] (a) P. Batten, A. Hamilton, A.W. Johnson, G. Shelton, D.J. Ward, Chem. Soc. Chem. Commun. (1974) 550–551;
(b) A.W. Johnson, D. Ward, P. Batten, A.L. Hamilton, G. Shelton, C.M. Elson, J. Chem. Soc. Perkin Trans. I (1975) 2076–2085;
(c) A.W. Johnson, D. Ward, J. Chem. Soc. Perkin Trans. I (1977) 720–723;
(d) P. Batten, A.L. Hamilton, A.W. Johnson, M. Mehendran, D. Ward, T.J. King, J. Chem. Soc. Perkin Trans. I (1977) 1623–1628.
[8] S.K. Koehn, S. Gronert, J.T. Aldajaei, Org. Lett. 12 (2010) 676–679.
[9] (a) T. Ikeno, I. Iwakura, T. Yamada, J. Am. Chem. Soc. 124 (2002) 15152–15153;
(b) I. Iwakura, H. Tanaka, T. Ikeno, T. Yamada, Chem. Lett. 33 (2004) 140–141.
[10] (a) W.I. Dzik, X. Xu, X.P. Zhang, J.N.H. Reek, B. de Bruin, J. Am. Chem. Soc. 132 (2010) 10891–10902;
(b) H. Lu, W.I. Dzik, X. Xu, L. Wojtas, B. de Bruin, X.P. Zhang, J. Am. Chem. Soc. 133 (2011) 8518–8521;
(c) N.D. Paul, A. Chirila, H. Lu, X.P. Zhang, B. de Bruin, Chem. Eur. J. 19 (2013) 12953.
[11] (a) A. Chirila, B.G. Das, N.D. Paul, B. de Bruin, ChemCatChem 9 (2017) 1413;
(b) B.G. Das, A. Chirila, M. Tromp, J.N.H. Reek, B. de Bruin, J. Am. Chem. Soc. 138 (2016) 8968.
[12] (a) D.G. Blackmond, Angew. Chem. Int. Ed. 44 (2005) 4302–4320;
(b) D.G. Blackmond, J. Am. Chem. Soc. 137 (2015) 10852–10866.
[13] (a) J. Eilmes, Polyhedron 10 (1991) 1779–1785;
(b) S.J. Dzugan, D.H. Busch, Inorg. Chem. 29 (1990) 2528–2532;
(c) J. Eilmes, Polyhedron 4 (1985) 943–946;
(d) J.H. Niewahner, K.A. Walters, A. Wagner, J. Chem. Ed. 84 (2007) 477;
(e) J.R. Chipperfield, S. Woodward, J. Chem. Ed. 71 (1994) 75–76.
[14] TURBOMOLE Version 6.5 (TURBOMOLE Gmbh, Karlsruhe, Germany, 2013).
[15] (a) PQS version 2.4, 2001, Parallel Quantum Solutions, Fayetteville, Arkansas, USA (the Baker optimizer is available separately from PQS upon request); (b) J. Baker, J. Comput. Chem. 7 (1986) 385–395.
[16] P.H.M. Budzelaar, J. Comput. Chem. 28 (2007) 2226.
[17] (a) A.D. Becke, Phys. Rev. A 38 (1988) 3098–3100;
(b) J.P. Perdew, Phys. Rev. B 33 (1986) 8822–8824.
[18] (a) F. Weigend, R. Ahlrichs, Phys. Chem. Chem. Phys. 7 (2005) 3297–3305;
(b) F. Weigend, M. Häser, H. Patzelt, R. Ahlrichs, Chem. Phys. Lett. 294 (1998) 143–152.
[19] In solution the catalyst is completely surrounded by solvent molecules, leading to small translational entropy contributions to the toluene molecule association/dissociation steps. These are of little influence on the translational entropy contributions associated with substrate/product association/dissociation. Hence, the latter are not canceled by the former in toluene solution.
[20] P.F. Kuijpers, M.J. Tiekink, W.B. Breukelaar, D.L.J. Broere, N.P. van Leest, J.I. van der Vlugt, J.N.H. Reek, B. de Bruin, Chem. Eur. J. 23 (2017) 7945–7952.
[21] W.I. Dzik, X.P. Zhang, B. de Bruin, Inorg. Chem. 50 (2011) 9896–9903.
[22] M. Goswami, A. Chirila, C. Rebreyend, B. de Bruin, Top. Catal. 58 (12–13) (2015) 719–750.
[23] G.R. Buettner, Free Radic. Biol. Med. 3 (1987) 259–303.
[24] (a) B. Walter, Z. Alessandro Del, P. Rigo, Chem. Commun. 86 (1997) 2163–2164;
(b) P.R. Krishna, R.S. Empati, F. Mongin, Tetrahedron Lett. 49 (2008) 6768–6772.